Determination of bed elevation in the enhanced lattice Boltzmann method for the shallow-water equations

Jian Guo Zhou[1,*] and Haifei Liu[2,†]

[1]*School of Engineering, University of Liverpool, Liverpool L69 3GQ, United Kingdom*

[2]*School of Environment, Beijing Normal University, Beijing 100875, People's Republic of China*

(Received 5 March 2013; revised manuscript received 10 May 2013; published 14 August 2013)

The bed slope in the shallow-water equations reflects the bed topography. It is not a flow variable and cannot be determined in the solution to the flow equations. An immovable nonflat bed affects a flow as a force term, but the flow has no effect on it. Only when the bed term is correctly represented in a numerical method can it generate an accurate solution. In the enhanced lattice Boltzmann method for the shallow-water equations (eLABSWE), using an individual Chapman-Enskog analysis, it is found that such a correct representation can be achieved by retaining $C_\alpha = 2\lambda_\alpha$, in which C_α is the coefficient for bed elevation in the lattice Boltzmann equation and λ_α is that for the water depth in the local equilibrium distribution function. The finding has been validated through simulations of a water at rest in a dish-shaped lake, a wind-induced shallow flow in the same lake, and a steady flow over a two-dimensional bed hump.

DOI: 10.1103/PhysRevE.88.023302 PACS number(s): 47.11.−j

Many practical flows have a common feature, i.e., the horizontal characteristics are dominant compared to the vertical, e.g., tidal flows, waves, open channel flows, dam breaks, and atmospheric flows. Such flows are called shallow-water flows and can be described by the shallow-water equations. Numerical solutions to the equations are an efficient practice to study a wide range of flow problems encountered in engineering [1–7]. Another peculiar property is that there is a bed slope in the equations that is a nonflow variable and determined by bed topography. Since natural flows always occur over a complex bed, an accurate treatment of the bed slope becomes the key to success or failure in a numerical method. For instance, in a Godunov-type method, a special treatment for bed slope has to be applied for accurate solutions [8–10]; in the lattice Boltzmann method for shallow-water equations (LABSWE), the use of the centered scheme for calculation of a bed slope is necessary to produce accurate solutions [7]; in the recent enhancement of the lattice Boltzmann method for shallow water equations (eLABSWE), the bed elevation is directly incorporated into the lattice Boltzmann equation to eliminate the requirement of calculating the derivative related to the bed slope. Although the centered scheme or the eLABSWE produces accurate solutions to most shallow-water flow problems, which is confirmed by van Thang *et al.* [11] in the theoretical analysis of the lattice Boltzmann method for a one-dimensional (1D) shallow-water equation, it is found that it fails to generate accurate solutions to some 2D shallow-water flows, such as a realistic wind-induced flow in a dish-shaped basin and a steady flow over a specific 2D hump. In this paper, we will show that such inaccuracy results from the mismatch between the coefficient for bed elevation in the lattice Boltzmann equation and that for the water depth in the local equilibrium distribution function. A correct relationship between the coefficients is proposed based on the individual Chapman-Enskog analysis. The scheme has been validated by simulating water at rest in a dish-shaped lake, a realistic wind-induced flow in the same lake, and a steady flow over a two-dimensional bed hump.

To improve the eLABSWE [12], we introduce a coefficient C_α into the lattice Boltzmann equation on a square lattice with nine particle velocities (D2Q9) as

$$\begin{aligned} f_\alpha(\mathbf{x}+\mathbf{e}_\alpha\Delta t, t+\Delta t) - f_\alpha(\mathbf{x},t) &= \frac{1}{\tau}\left(f_\alpha^{\mathrm{eq}} - f_\alpha\right) - C_\alpha\frac{g\overline{h}}{e^2}[z_b(\mathbf{x}+\mathbf{e}_\alpha\Delta t) - z_b(\mathbf{x})] \\ &\quad + \frac{\Delta t}{6e^2}e_{\alpha j}F_j, \end{aligned} \tag{1}$$

where f_α is the particle distribution function; $\mathbf{x}$ is the space vector defined by Cartesian coordinates, i.e., $\mathbf{x} = (x, y)$ in 2D space; t is the time; Δt is the time step; $\mathbf{e}_\alpha$ is the particle velocity vector; $e_{\alpha j}$ is the component of $\mathbf{e}_\alpha$ in the jth direction; $e = \Delta x/\Delta t$, Δx is the lattice size; z_b is the bed elevation above a datum; τ is the single relaxation time [13]; f_α^{eq} is the local equilibrium distribution function; C_α is a constant to be decided; $\overline{h} = 0.5[h(\mathbf{x}+\mathbf{e}_\alpha\Delta t, t+\Delta t) + h(\mathbf{x},t)]$; and

$$F_j = \frac{\tau_{wj}}{\rho} - \frac{\tau_{bj}}{\rho} + \Omega h u_y \delta_{jx} - \Omega h u_x \delta_{jy}, \tag{2}$$

in which h is the water depth, defined as the height from the bed to the water surface; u_i is the depth-averaged velocity; $g = 9.81\ \mathrm{m/s^2}$ is the gravitational acceleration; τ_{wj} is the wind shear stress in the jth direction; τ_{bj} is the bed shear stress in the jth direction defined by the depth-averaged velocities with a bed friction coefficient C_b as

$$\tau_{bj} = \rho C_b u_j \sqrt{u_i u_i}; \tag{3}$$

ρ is the water density; Ω is the Coriolis parameter for the effect of the earth's rotation; and δ_{ij} is the Kronecker delta function,

$$\delta_{ij} = \begin{cases} 0, & i \neq j, \\ 1, & i = j. \end{cases} \tag{4}$$

*J.G.Zhou@liverpool.ac.uk

†haifei.liu@bnu.edu.cn

We redefine a general local equilibrium distribution function with two unknown constants A and B as follows:

$$f_\alpha^{\rm eq} = \begin{cases} \left[1-4(A+B)\frac{gh}{e^2} - \frac{u_i u_i}{e^2}\right]h, & \alpha = 0, \\ \left(A\frac{gh}{e^2} + \frac{e_{\alpha_i} u_i}{3e^2} + \frac{(e_{\alpha_i} u_i)^2}{2e^4}\right)h, & \alpha = 1,3,5,7, \\ \left(B\frac{gh}{e^2} + \frac{u_i}{12e_{\alpha i}} + \frac{u_x u_y}{4e_{\alpha x} e_{\alpha y}}\right)h, & \alpha = 2,4,6,8, \end{cases} \tag{5}$$

where A and B satisfy the following constraint:

$$2A + 4B = \tfrac{1}{2}. \tag{6}$$

A and B can also be represented with λ_α defined as

$$\lambda_\alpha = \begin{cases} A, & \alpha = 1,3,5,7, \\ B, & \alpha = 2,4,6,8. \end{cases} \tag{7}$$

The physical variables of water depth and velocity are calculated by

$$h = \sum_\alpha f_\alpha \tag{8}$$

and

$$u_i = \frac{1}{h}\sum_\alpha e_{\alpha i} f_\alpha. \tag{9}$$

It can be shown following the Chapman-Enskog analysis described in the eLABSWE [12] that Eq. (1) can recover the following shallow-water equations:

$$\frac{\partial h}{\partial t} + \frac{\partial (h u_j)}{\partial x_j} = 0, \tag{10}$$

$$\frac{\partial (h u_i)}{\partial t} + \frac{\partial (h u_i u_j)}{\partial x_j} = -g\frac{\partial}{\partial x_i}\left(\frac{h^2}{2}\right) - gh\frac{\partial z_b}{\partial x_i} + \nu\frac{\partial^2 (h u_i)}{\partial x_j \partial x_j} + F_i, \tag{11}$$

on the condition that C_α satisfies

$$\sum_\alpha C_\alpha e_{\alpha i} e_{\alpha j} = e^2 \delta_{ij}. \tag{12}$$

It may be noted that the widespread use of the standard local equilibrium distribution function in the lattice Boltzmann method for the shallow-water equations is

$$f_\alpha^{\rm eq} = \begin{cases} h\left(1 - \frac{5gh}{6e^2} - \frac{2u_i u_i}{3e^2}\right), & \alpha = 0, \\ \omega_\alpha h\left(\frac{gh}{6e^2} + \frac{e_{\alpha i} u_i}{3e^2} + \frac{e_{\alpha i} e_{\alpha j} u_i u_j}{2e^4} - \frac{u_i u_i}{6e^2}\right), & \alpha \neq 0, \end{cases} \tag{13}$$

in which $\omega_\alpha = 1$ when $\alpha = 1,3,5,7$ and $\omega_\alpha = 1/4$ when $\alpha = 2,4,6,8$. Equation (13) can be derived in different ways. For example, Zhou [14] uses the basic constraints and lattice symmetry; Dellar [15] starts from the standard local equilibrium distribution function for the Navier-Stokes equation and derives it through applying nonhydrodynamic ghost variables; and Tubbs and Tsai [16] replace the density with water depth and redefine the sound speed C_s as $C_s = \sqrt{gh/2}$ with a little modification to the standard local equilibrium distribution function for the Navier-Stokes equation. The described equation (5) may be considered as an improved version of Eq. (13) as they are effectively the same except that (i) Eq. (5) can take different coefficients of the water depth for additional flexibility, and (ii) it contains no negative part related to the term $u_i u_i$ for $\alpha \neq 0$. Such a difference may make the eLABSWE an additional freedom to have better numerical stability when Eq. (5) is applied.

For further analysis, we recall the $\mathcal{N}$ property: A numerical scheme is said to satisfy the *necessary property* ($\mathcal{N}$ property) provided that it can replicate the exact solution to a stationary case $u_i \equiv 0$ in which there is a nonzero force or source term [7]. For example, in the shallow-water equations there is a nonzero bed slope, which is represented with the bed level in Eq. (1). Many different numerical studies [8–10] show that an inappropriate treatment for this term can produce results with large errors, and particularly artificial flows for water at rest in a container with a nonflat bed. Consequently, formulating a numerical scheme that satisfies the $\mathcal{N}$ property is the fundamental requirement for an accurate solution. In physics, the water level $z_b + h$ above a datum is independent of bed topography when water stays still. As for the water at rest in a container with an uneven bottom, there is an exact solution, i.e., $u_i \equiv 0$ and $h + z_b \equiv const$. Without loss of generality, this case can be used to find the correct relationship between C_α and λ_α through the Chapman-Enskog analysis. Assuming that Δt is small and

$$\Delta t = \varepsilon, \tag{14}$$

we have Eq. (1) expressed as

$$f_\alpha(\mathbf{x} + \mathbf{e}_\alpha \varepsilon, t + \varepsilon) - f_\alpha(\mathbf{x}, t) = -\frac{1}{\tau}\left(f_\alpha - f_\alpha^{\rm eq}\right) - C_\alpha \frac{g\overline{h}}{e^2}[z_b(\mathbf{x} + \mathbf{e}_\alpha \varepsilon) - z_b(\mathbf{x})] + \frac{\varepsilon}{6e^2} e_{\alpha j} F_j. \tag{15}$$

Taking a Taylor expansion to the first term on the left-hand side of the above equation in time and space at point $(\mathbf{x},t)$ leads to

$$\varepsilon\left(\frac{\partial}{\partial t} + e_{\alpha j}\frac{\partial}{\partial x_j}\right) f_\alpha + \frac{\varepsilon^2}{2}\left(\frac{\partial}{\partial t} + e_{\alpha j}\frac{\partial}{\partial x_j}\right)^2 f_\alpha + O(\varepsilon^3). \tag{16}$$

According to the Chapman-Enskog procedure, f_α can be expanded around $f_\alpha^{(0)}$,

$$f_\alpha = f_\alpha^{(0)} + \varepsilon f_\alpha^{(1)} + \varepsilon^2 f_\alpha^{(2)} + O(\varepsilon^3). \tag{17}$$

The second term on the right-hand side of Eq. (15) can also be expressed via the Taylor expansion,

$$C_\alpha \frac{g}{e^2}\left[h + \frac{\varepsilon}{2}\left(\frac{\partial h}{\partial t} + e_{\alpha j}\frac{\partial h}{\partial x_j}\right)\right] \times \left(\varepsilon e_{\alpha j}\frac{\partial z_b}{\partial x_j} + \frac{\varepsilon^2}{2} e_{\alpha i} e_{\alpha j}\frac{\partial^2 z_b}{\partial x_i \partial x_j}\right) + O(\varepsilon^3). \tag{18}$$

The centered scheme [7] is used for the force term F_j,

$$F_j = F_j\left(\mathbf{x} + \tfrac{1}{2}\mathbf{e}_\alpha \varepsilon, t + \tfrac{1}{2}\varepsilon\right), \tag{19}$$

which can again be written, via a Taylor expansion, as

$$F_j\left(\mathbf{x} + \frac{1}{2}\mathbf{e}_\alpha \varepsilon, t + \frac{1}{2}\varepsilon\right) = F_j + \frac{\varepsilon}{2}\left(\frac{\partial F_j}{\partial t} + e_{\alpha i}\frac{\partial F_j}{\partial x_i}\right) + O(\varepsilon^2). \tag{20}$$

After inserting Eqs. (16), (17), (18), and (20) into Eq. (15), equating the coefficients of ε^0 and ε leads to

$$f_\alpha^{(0)} = f_\alpha^{\mathrm{eq}} \tag{21}$$

and

$$\left(\frac{\partial}{\partial t} + e_{\alpha j}\frac{\partial}{\partial x_j}\right) f_\alpha^{(0)} = -\frac{f_\alpha^{(1)}}{\tau} - C_\alpha \frac{g h e_{\alpha j}}{e^2}\frac{\partial z_b}{\partial x_j} + \frac{e_{\alpha j} F_j}{6e^2}. \tag{22}$$

Applying the exact solution of $u = 0$ and $h + z_b = \text{const}$ for the water at rest to Eq. (22) yields

$$\frac{\partial}{\partial x_j}\left(e_{\alpha j} f_\alpha^{(0)}\right) = -\frac{f_\alpha^{(1)}}{\tau} - C_\alpha \frac{g h e_{\alpha j}}{e^2}\frac{\partial z_b}{\partial x_j}. \tag{23}$$

Multiplying the above equation by $e_{\alpha i}$ gives

$$\frac{\partial}{\partial x_j}\left[e_{\alpha i} e_{\alpha j} f_\alpha^{(0)}\right] = -\frac{e_{\alpha i} f_\alpha^{(1)}}{\tau} - C_\alpha \frac{g h e_{\alpha i} e_{\alpha j}}{e^2}\frac{\partial z_b}{\partial x_j}. \tag{24}$$

As van Thang *et al.* [11] analytically show that $f_\alpha^{(\mathrm{neq})} = 0$ for a stationary flow over a 1D nonflat bed, we may also assume that $f_\alpha^{(1)}$ can be treated as zero in the 2D case for the following analysis, leading to

$$\frac{\partial}{\partial x_j}\left[e_{\alpha i} e_{\alpha j} f_\alpha^{(0)}\right] = -C_\alpha \frac{g h e_{\alpha i} e_{\alpha j}}{e^2}\frac{\partial z_b}{\partial x_j}, \tag{25}$$

which generates little error in the simulation as its accumulative first momentum has no effect on the macroscopic equation due to $\sum e_{\alpha i} f_\alpha^{(1)} = 0$. Substitution of Eq. (5) into the above provides

$$\lambda_\alpha \frac{g}{e^2}\frac{\partial}{\partial x_j}(e_{\alpha i} e_{\alpha j} h^2) = -C_\alpha \frac{g h e_{\alpha i} e_{\alpha j}}{e^2}\frac{\partial z_b}{\partial x_j}. \tag{26}$$

If we choose

$$C_\alpha = 2\lambda_\alpha = \begin{cases} 2A, & \alpha = 1,3,5,7, \\ 2B, & \alpha = 2,4,6,8, \end{cases} \tag{27}$$

which automatically satisfies the condition (12), Eq. (26) can be written as

$$2\lambda_\alpha e_{\alpha i} e_{\alpha j}\frac{\partial}{\partial x_j}(h + z_b) = 0, \tag{28}$$

which holds true due to the exact solution of $h + Z_b = \text{const}$ for the water at rest. Thus Eq. (27) is the correct link between C_α and λ_α to retain an accurate solution in the eLABSWE.

As the dropped small term $f_\alpha^{(1)}$ in the above derivation has no effect on the accumulative mass and momentum, such a relationship ensures that the $\mathcal{N}$ property is exactly satisfied in the recovered flow equations at the macroscopic level. In the standard local equilibrium distribution function (13) for the shallow-water equations, we have

$$\lambda_\alpha = \begin{cases} A = 1/6, & \alpha = 1,3,5,7, \\ B = 1/24, & \alpha = 2,4,6,8; \end{cases} \tag{29}$$

and hence Eq. (27) is applied to determine C_α as

$$C_\alpha = \begin{cases} 2A = 1/3, & \alpha = 1,3,5,7, \\ 2B = 1/12, & \alpha = 2,4,6,8 \end{cases} \tag{30}$$

for accurate solutions to shallow-water flows over uneven beds.

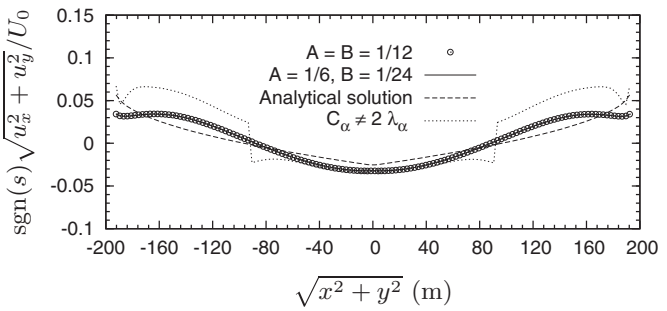

FIG. 1. Comparison of the resultant velocities along cross-section *A-A* with the slip boundary condition (see Fig. 2) and $U_0 = 0.129$ m/s, $s = u_x + u_y$.

It must be pointed that (a) if the condition (27) is violated, e.g., $C_\alpha = 1/6$ with λ_α given by Eq. (29), i.e., $C_\alpha \neq 2\lambda_\alpha$, the lattice Boltzmann equation (1) can still recover the correct macroscopic shallow-water equations (10) and (11), but it fails to generate accurate solutions to 2D shallow-water flows over uneven beds due to the fact that it does not satisfy the $\mathcal{N}$ property, which is further confirmed by the following numerical tests; and (b) in the original eLABSWE or the centered scheme, $C_\alpha = 1/6$ [7], which can produce accurate solutions only on the condition that $A = B = 1/12$, or λ_α is defined as

$$\lambda_\alpha = \begin{cases} A = 1/12, & \alpha = 1,3,5,7, \\ B = 1/12, & \alpha = 2,4,6,8, \end{cases} \tag{31}$$

which satisfies the condition (27) and is again supported by the following numerical tests, indicating that the eLABSWE or the centered scheme is just one special case of many combinations using Eqs. (6) and (27).

To verify the described scheme, three numerical tests are presented, where the SI units are used for the physical variables. Additionally, $\overline{h}$ is determined using the following semi-implicit form:

$$\overline{h} = 0.5[h(\mathbf{x} + \mathbf{e}_\alpha \Delta t, t) + h(\mathbf{x}, t)], \tag{32}$$

which is simple and demonstrated to produce accurate solutions in the eLABSWE [12]. First of all, a 2D stationary case is

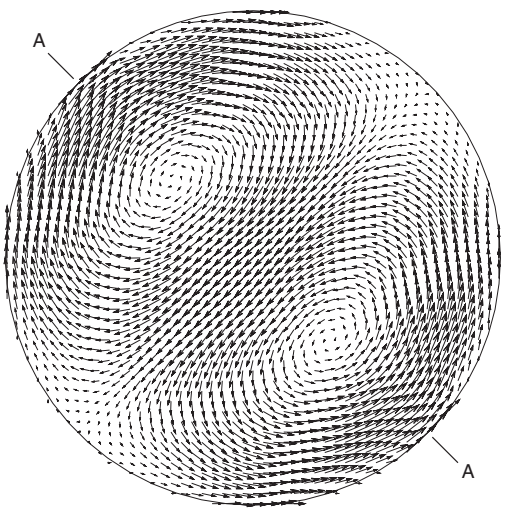

FIG. 2. Correct flow pattern when $C_\alpha = 2\lambda_\alpha$.

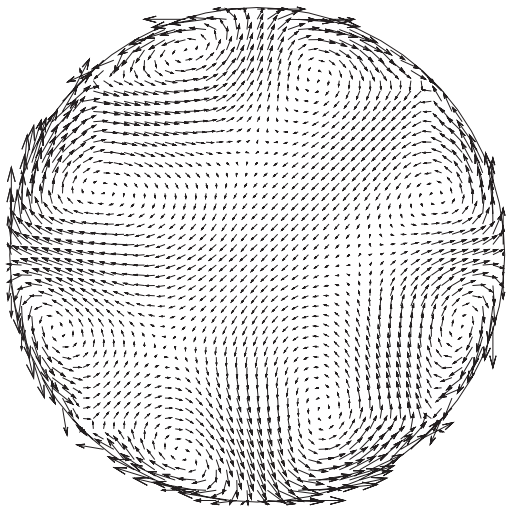

FIG. 3. Wrong flow pattern when $C_\alpha \neq 2\lambda_\alpha$.

considered in a circular basin with bed topography described using the still water depth H with the coordinate origin at the basin center,

$$H(x,y) = \frac{1}{1.3}\left(\frac{1}{2} + \sqrt{\frac{1}{2} - \frac{\sqrt{x^2+y^2}}{386.4}}\right), \tag{33}$$

which is the same basin used by Rogers *et al.* [17] and Zhou [18]; the bed level can be determined as $z_b(x,y) = H(0,0) - H(x,y)$. This case is used to examine if the proposed scheme satisfies the $\mathcal{N}$ property. 200×200 lattices are used together with $\Delta x = 2$, $\Delta t = 0.2$, and $\tau = 1.3$ in simulations. The bounce-back scheme is used for the no-slip boundary condition at the basin boundary. We have tested this case using the two sets of coefficients λ_α given by Eqs. (29) and (31). Using C_α defined by Eq. (27), the simulation shows that the numerical results remain an exact stationary state with machine accuracy for any running period, confirming that the scheme satisfies the $\mathcal{N}$ property [7]. The solution is independent of the choices of the coefficient λ_α as long as the conditions (6) and (27) are satisfied. However, if $C_\alpha = 1/6$ is used for λ_α given by Eq. (29) for this test, it turns out that the model produces results at a maximum artificial velocity of 0.0026 m/s, failing to retain the exact solution to this 2D water at rest because it violates the condition (27), i.e., it does not satisfy the $\mathcal{N}$ property.

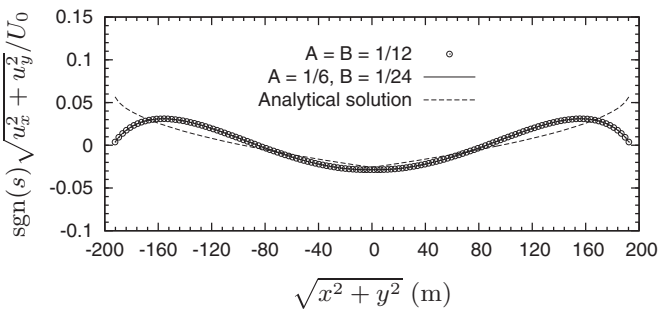

FIG. 4. Comparison of the resultant velocities along cross-section A-A with the no-slip boundary condition (see Fig. 2) and $U_0 = 0.129$ m/s, $s = u_x + u_y$.

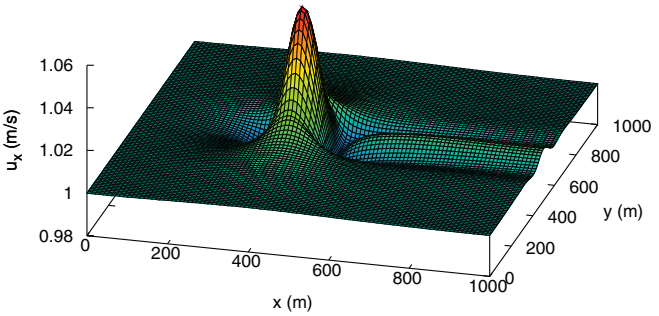

FIG. 5. (Color online) Correct velocity u_x distribution when $C_\alpha = 2\lambda_\alpha$.

Secondly, we consider a wind-driven circulation in the same lake defined by Eq. (33). This may generate a complex flow phenomenon [19]. The wind shear stress may generally be defined as

$$\tau_w = \rho_a C_w u_w^2, \tag{34}$$

in which $\rho_a = 1.293$ kg/m^3, u_w is the wind speed, and $C_w = 0.0026$. For this test, a uniform wind speed of $u_w = 5$ m/s blows from the southwest to the northeast and the components of the wind shear stress are

$$(\tau_{wx}, \tau_{wy}) = \tau_w\left(\cos\frac{\pi}{4}, \sin\frac{\pi}{4}\right). \tag{35}$$

According to the theoretical analysis [19], the steady flow consists of two relatively strong counterrotating gyres with flow in the deeper water against the direction of the wind, exhibiting a complex flow phenomenon. In the numerical simulation, the same computational parameters as those for the stationary test together with slip and no-slip boundary conditions are used. For the slip boundary condition, the elastic-collision scheme is used [7]. Again, Eqs. (29) and (31) are used for λ_α together with Eq. (27) for C_α. After the steady solutions are obtained, the comparisons of the normalized resultant velocities at cross section A-A with each other are depicted in Fig. 1, indicating that both generate the same results, which are further compared to the analytical solution in the same plot, demonstrating similar accuracy to that reported in the literature [17,18]. The flow field is plotted in Fig. 2, showing the correct flow pattern. Despite the comparable results, there is a discrepancy between the numerical predictions and the analytical solution. This is due to the fact that (a) the assumptions of both the rigid-lid approximation for the water surface and a parabolic

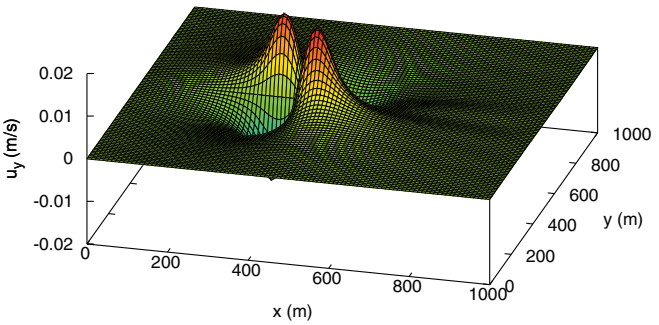

FIG. 6. (Color online) Correct velocity u_y distribution when $C_\alpha = 2\lambda_\alpha$.

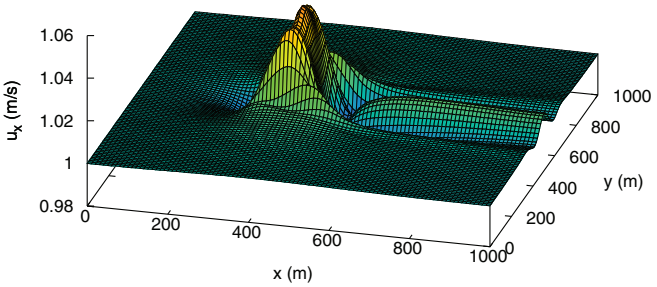

FIG. 7. (Color online) Wrong velocity u_x distribution when $C_\alpha \neq 2\lambda_\alpha$.

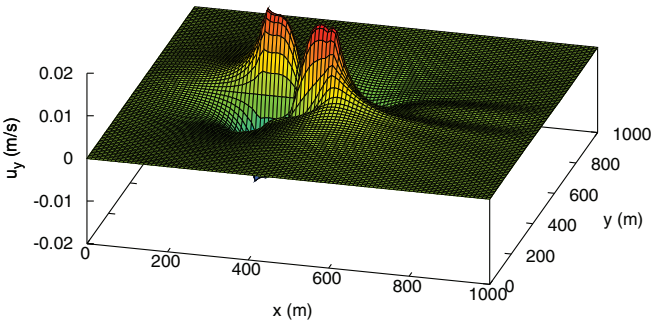

FIG. 8. (Color online) Wrong velocity u_y distribution when $C_\alpha \neq 2\lambda_\alpha$.

distribution for the eddy viscosity were used in the analytical solution, and (b) the effect of turbulence on flow is not taken into account in the numerical computations. Similarly, if $C_\alpha = 1/6$ is used with the λ_α value given by Eq. (29), the model yields an inaccurate solution as compared in Fig. 1 and also shows a wrong flow pattern as plotted in Fig. 3 because of $C_\alpha \neq 2\lambda_\alpha$. This confirms that any combination of the coefficients C_α and λ_α satisfying both Eqs. (6) and (27) will generate the right numerical solutions. The results using no-slip boundary conditions are also compared with the analytical solution in Fig. 4, from which it is clearly seen that a large difference exists in the vicinity of the boundary as it is contradictory to the use of the slip boundary condition in the analytical solution.

Finally, a steady shallow-water flow over a 2D hump is investigated. The 2D hump is defined as

$$z_b(x,y) = \begin{cases} \psi(x,y) & \text{if } (x,y) \in \Omega, \\ 0 & \text{otherwise}, \end{cases} \tag{36}$$

where $\Omega = [300,500] \times [400,600]$ and

$$\psi(x,y) = \sin^2\left(\frac{\pi(x-300)}{200}\right)\sin^2\left(\frac{\pi(y-400)}{200}\right). \tag{37}$$

The flow conditions are as follows: discharge per unit width is $q = 10$ m^2/s, water depth is $h = 10$ m at the outflow boundary, and the channel is 1000 m long and 1000 m wide. This is the same test as that used by researchers in validation of numerical methods [20–22] for sediment transport under shallow-water flows. Here only steady flow over the fixed bed without sediment transport is simulated, as prediction of correct flow plays an essential role in the determination of bed evolution, and hence it is a suitable test for the proposed scheme. We use 200×200 lattices together with $\Delta x = 5$ and $\Delta t = 0.1$. After the steady solutions are obtained, the results using the same two sets of C_α and λ_α as those in the previous tests are presented. The velocities u_x and u_y are shown in Figs. 5 and 6, respectively, demonstrating the right velocity distributions in good agreement with those obtained using high-resolution Godunov-type numerical methods [20–22]. For comparison, we also run this case using $C_\alpha = 1/6$ for λ_α given by Eq. (29). The velocities u_x and u_y are shown in Figs. 7 and 8, demonstrating the wrong velocity distributions over the top of the hump, which are very different from the correct velocity distributions.

In conclusion, an internal correct link between the coefficient for the bed elevation C_α and that for the water depth in the local equilibrium distribution function λ_α is discovered through the individual Chapman-Enskog analysis. This changes the way of applying the Chapman-Enskog analysis to formulating an accurate lattice Boltzmann scheme for a physical phenomena, i.e., the right individual formulation for each lattice direction based on a special case can result in an accurate solution at the macroscopic level. On the other hand, an LBM that recoveries the correct macroscopic flow equations may not produce accurate results, which has been confirmed in the present research. The descried relationship provides an accurate scheme to represent the bed topography as a nonflow parameter in the eLABSWE. Numerical tests have demonstrated that $C_\alpha = 2\lambda_\alpha$ in the eLABSWE can ensure accurate solutions, making it an ideal model for simulating complex shallow-water flows in practice.

The financial support from the National Basic Research Program of China (973) (2011CB403304) and the National Natural Science Foundation of China (51009007) are gratefully acknowledged.

[1] A. Alcrudo and P. Garcia-Navarro, Int. J. Numer. Methods Fluids **16**, 489 (1993).
[2] V. Casulli, J. Comput. Phys. **86**, 56 (1990).
[3] C. B. Vreugdenhil, *Numerical Methods for Shallow-water Flow* (Kluwer Academic, Dordrecht, 1994).
[4] A. G. L. Borthwick and G. A. Akponasa, J. Hydr. Eng. Div., ASCE **123**, 432 (1997).
[5] B. Yulistiyanto, Y. Zech, and W. H. Graf, J. Hydraul. Eng., ASCE **124**, 419 (1998).
[6] K. Hu, C. G. Mingham, and D. M. Causon, Coastal Eng. **41**, 433 (2000).
[7] J. G. Zhou, *Lattice Boltzmann Methods for Shallow Water Flows* (Springer-Verlag, Berlin, 2004).
[8] A. Bermudez and M. E. Vázquez, Comput. Fluids **23**, 1049 (1994).
[9] R. J. LeVeque, J. Comput. Phys. **146**, 346 (1998).
[10] J. G. Zhou, D. M. Causon, C. G. Mingham, and D. M. Ingram, J. Comput. Phys. **168**, 1 (2001).

[11] P. van Thang, B. Chopard, L. Lefèvre, D. A. Ondo, and E. Mendes, J. Comput. Phys. **229**, 7373 (2010).
[12] J. G. Zhou, J. Comput. Phys. **230**, 394 (2011).
[13] P. L. Bhatnagar, E. P. Gross, and M. Krook, Phys. Rev. **94**, 511 (1954).
[14] J. G. Zhou, Comput. Methods Appl. Mech. Eng. **191**, 3527 (2002).
[15] P. J. Dellar, Phys. Rev. E **65**, 036309 (2002).
[16] K. R. Tubbs and F. T. C. Tsai, Adv. Water Resourc. **32**, 1767 (2009).
[17] B. Rogers, M. Fujihara, and A. G. L. Borthwick, Int. J. Numer. Methods Fluids **35**, 247 (2001).
[18] J. G. Zhou, Int. J. Mod. Phys. C **12**, 387 (2001).
[19] C. Kranenburg, J. Hydr. Res. **30**, 29 (1992).
[20] J. Hudson and P. K. Sweby, Int. J. Numer. Methods Fluids **47**, 1085 (2005).
[21] J. Huang, A. G. L. Borthwick, and R. L. Soulsby, Proc. Inst. Civil Eng.: J. Eng. Computat. Mech. **163**, 101 (2010).
[22] F. Benkhaldoun, S. Sahmim, and M. Seaïd, Int. J. Numer. Methods Fluids **63**, 1296 (2010).